# *Ab initio* calculation of the electronic, structural, and dynamical properties of AlAs and CdTe

Bal K. Agrawal and Savitri Agrawal
*Physics Department, Allahabad University, Allahabad 211002, India*
(Received 13 August 1991)

The scalar-relativistic version of an accurate first-principles full-potential self-consistent linearized muffin-tin-orbital (LMTO) method has been employed for describing the physical properties of the III-V and II-VI semiconducting compounds. Results for the two prototypes, AlAs and CdTe, are presented. The presently employed modified version of the LMTO method is quite fast and goes beyond the usual LMTO-atomic-sphere-approximation (ASA) method in the sense that it permits a completely general shape of the potential and the charge density. Also, in contrast to LMTO-ASA, the present method is capable of treating distorted lattice structures accurately. The calculated value of the lattice parameter is equal to the experimental value for the III-V compound AlAs and lies within 2.5% of the measured value for the II-VI compound CdTe. The computed density of states is quite close to the photoemission data available for CdTe. The calculated values of the bulk modulus and the elastic constants are in good agreement with the experimental data except for $C_{44}$ in CdTe. The values of the phonon frequencies at some symmetry points are also in close agreement with the experimental data wherever available. The present method is thus capable of predicting many physical properties of the polar semiconductors both qualitatively and quantitatively.

## I. INTRODUCTION

In the past decade it has been observed that the structural and lattice-dynamical properties can be determined *ab initio* with reliable accuracy if one can calculate the electronic energy of the solid as a function of the atomic positions using the usual density-functional theory.

Recently, the linear-muffin-tin orbital (LMTO) method has drawn much attention towards its application to the study of the electronic structure of molecules as well as of crystalline solids. The method has several advantages, (i) Only a minimal basis set is required in the method, thus it enables its application to large unit cells with high efficiency. (ii) The method treats all the elements of the Periodic Table in a similar manner. Thus the atoms with a large number of core states and the metals having prominently $d$ or $f$ character can be treated easily. (iii) As the augmentation procedure generates the correct shape of the wave function near the nuclei, it is quite accurate. (iv) The use of atom-centered basis functions belonging to the different values of the angular momentum in the method helps one to have a quite clear physical picture.

Usually in the application of the standard LMTO method, an atomic sphere approximation (ASA) is used to make it efficient. However, this LMTO-ASA method suffers from several disadvantages. (i) It neglects the symmetry-breaking terms by discarding the nonspherical parts of the electron density. (ii) The method discards the interstitial region by replacing the muffin-tin spheres by space-filling Wigner spheres. (iii) It uses spherical Hankel functions with vanishing kinetic energy.

It has been noted that quite reliable results could be attained by employing a LMTO basis set if all the potential terms are determined accurately. For this the sizes of the atomic spheres are shrunk so as to make them nonoverlapping. The potential matrix elements are then split into two parts, one contribution coming from the atomic spheres and the other from the complicated interstitial region. The first part, i.e., the atomic sphere one, is easy to evaluate by expanding it in terms of the usual spherical harmonics. On the other hand, the evaluation of the interstitial contribution is quite difficult and very time-consuming if done by standard techniques. Efforts have been made to find an efficient and quick way to determine the interstitial contribution. In the method used in the present work, the interstitial quantities were expanded in terms of the spherical Hankel functions. The involved three-center integrals were expressed as the linear combination of the two-center integrals by numerical means. These two-center integrals involving Hankel functions can easily be evaluated analytically. The method does not employ the plane waves and is thus applicable to the periodic as well as the nonperiodic systems which so often need to be treated especially when there occur impurities, defects, and the lattice distortions or atomic relaxations.

The present LMTO method is seen to produce the electronic structure, cohesive energy, lattice constants, elastic constants, phonon frequencies, mode Grüneisen and strain parameters for the simple systems like Si, C, etc.[1-3] Very recently, the method has been successfully applied also for the III-V and II-VI semiconducting compounds like AlAs, CdS, GaSb, ZnSe, ZnTe, ZnS, etc. The influence of structural relaxation of the atoms on the valence-band offset at the lattice matched interfaces of II-VI and III-V semiconductors ZnTe/GaSb (110) and the lattice mismatched interface ZnS/ZnSe (001) has been investigated.[4]

 

We have employed a scalar relativistic version of an accurate and fast first-principles full-potential self-consistent LMTO method for the calculation of the electronic structure, statical and dynamical properties of the III-V and II-VI semiconducting compounds. Section II contains a brief summary of the modifications employed in the present version of the method using Hankel functions. This section also includes a brief discussion of the internal energy after deformation and the evaluation of elastic constants. The results for the two prototypes of the III-V and II-VI semiconductors, i.e., AlAs and CdTe, are presented in Sec. III. The main conclusions are included in Sec. IV.

## II. METHOD

One needs to evaluate the interstitial potential matrix elements

$$V^I_{nL,n'L'}=\int_I \chi^*_{nL}(\mathbf{r})V_I(\mathbf{r})\chi_{n'L'}(\mathbf{r})d\mathbf{r}\ . \tag{1}$$

Here, $I$ denotes the interstitial region having the potential $V_I$, $\chi_{nL}$ denotes a LMTO envelope function centered at the site $n$ with angular momentum $L$, and the integration is over the volume element $d\mathbf{r}$ to be done in the interstitial region. Here $L$ denotes the angular momentum quantum number set $(l,m_L)$, etc.

The above problem is related to finding a tractable form of the output charge density in the interstitial region which is expressed as a linear combination of the products $\chi^*_{nL}\chi_{n'L'}$. In the present method a linear combination of atom-centered Hankel functions of negative energy is fitted to the charge density. As the contribution of the higher angular-momentum varies quite strongly, one may employ a cutoff.

In the interstitial region one determines the coefficients of the linear expansion

$$\chi^*_{nL}(\mathbf{r})\chi_{n'L'}(\mathbf{r})\approx\sum_{\mu,K,\alpha}A^{nLn'L'}_{\mu K\alpha}H_{\mu K\alpha}(\mathbf{r})\ , \tag{2}$$

where

$$H_{\mu K\alpha}(\mathbf{r})=h_K(i\lambda_\alpha|\mathbf{r}-\mathbf{R}_\mu|)Y_K[(\mathbf{r}-\mathbf{R}_\mu)/|\mathbf{r}-\mathbf{R}_\mu)|] \tag{3}$$

Here the functions $H_{\mu K\alpha}$'s have a general form similar to LMTO envelope functions and $h_K$'s and $Y_K$'s are the atom-centered Hankel and spherical harmonics, respectively.

The coefficients $A$'s in Eq. (2) have to be determined numerically. The substitution of the expansion (2) in Eq. (1) reduces the matrix elements into a linear combination of integrals of the functions $H_{\mu K\alpha}$ times the interstitial potential which itself can be expanded into functions of $H_{\mu K\alpha}$ type. This procedure is convenient because the Poisson equation can be solved analytically in the Hankel-function basis. Hence the three-center integrals of Eq. (1) have now been expressed as a linear combination of integrals of products of pairs of Hankel functions. Employing Gauss's theorem and the fact that $H_{\mu K\alpha}$ are eigenfunctions of the Laplace operator, the two-center integrals can be expressed as surface integrals over the spheres which are easy to evaluate by structure-constant expansions.

We then make the one-center expansion near the site $\mu$,

$$\chi_{nL}(\mathbf{r})=\sum[a^{nL}_{\mu K}H_{\mu K}(\mathbf{r})+b^{nL}_{\mu K}J_{\mu K}(\mathbf{r})]\ , \tag{4}$$

where $H_{\mu K}$ is given as in Eq. (3) and $J_{\mu K}$ is defined in a similar way for the spherical Bessel function both at the same kinetic energy as $\chi_{nL}$.

For the interstitial matrix elements one can then write

$$\begin{aligned}\int_i\chi^*_{nL}(\mathbf{r})V_I(\mathbf{r})\chi_{n'L'}(\mathbf{r})d\mathbf{r}&=\sum(a^{nL*}_{\mu K}D^{HH}_{\mu KK'}a^{n'L'}_{\mu K'}+a^{nL*}_{\mu K}D^{HJ}_{\mu KK'}b^{n'L'}_{\mu K'}\\&\quad+b^{nL*}_{\mu k}D^{JH}_{\mu KK'}a^{n'L'}_{\mu K'}+b^{nL*}_{\mu K}D^{JJ}_{\mu KK'}b^{n'L'}_{\mu K'})\ .\end{aligned} \tag{5}$$

Here $D$'s are matrices which are all $k$ independent.

For the evaluation of the nonspherical potential terms inside the atomic spheres, one obtains an expression of form similar to Eq. (5) with the $D_{\mu KK'}$ replaced by the integrals which give the coupling between the augmented "heads" and "tails" on the $\mu$th sphere. Hence once the matrices in Eq. (5) are determined, the corrections to the muffin-tin potential from inside the spheres and from the interstitial can be treated together. The full-potential calculation thus reduces to the evaluation of the effect of nonspherical potential in the spheres.

### Elastic constants

The change in the total energy with distortion may be utilized to evaluate the elastic constants of a solid. For uniform deformation let a lattice point at $\mathbf{R}$ in any undistorted Bravis lattice be shifted to a new lattice point $\mathbf{R}'$ in the distorted lattice. The Cartesian components can be described by

$$R_i'=\sum_{i=1}^{3}\alpha_{ij}R_j\ . \tag{6}$$

The matrix $\{\alpha_{ij}\}$ is then given by its elements,

$$\alpha_{ij}=\delta_{ij}+\epsilon_{ij}\ . \tag{7}$$

The strain tensor $(e_{ij})$ is defined as

$$e_{ij}=\epsilon_{ij}+\epsilon_{ji}(1-\delta_{ij})\ . \tag{8}$$

One may expand the internal energy of a distorted solid per unit-cell volume $V_0$ ($V_0$ being the unit-cell volume of the undistorted lattice) in powers of the components of the strain tensor $\{e_{ij}\}$ as

$$E(e)=E(0)+\sum_{i,j}\tau_{ij}e_{ij}+\tfrac{1}{2}\sum_{i,j}\sum_{k,l}c_{ijkl}e_{ij}e_{kl}+\cdots\ , \tag{9}$$

where $E(0)$ is the internal energy of the undistorted lattice; $\tau_{ij}=(\partial E/\partial e_{ij})_0$ is the first energy derivating tensor and $c_{ijkl}=(\partial^2E/\partial e_{ij}\partial e_{kl})_0'$ are the second-order adiabatic elastic constants. A subscript "0" on the parentheses denotes that all the strains except the $e_{ij}$ or $e_{ij}e_{kl}$ are kept constant while differentiating with respect to $e_{ij}$ or $e_{ij}$ and $e_{kl}$, respectively. After utilizing the symmetry properties of the individual tensors and the standard notation $11\equiv1$, $22\equiv2$, $33\equiv3$, $23\equiv4$, $31\equiv55$, and $12\equiv6$, Eq. (9)

has the simple form

$$E(\epsilon)=E(0)+\sum_i \tau_i e_i+\tfrac{1}{2}\sum_{i,j} c_{ij}e_i e_j+\cdots . \quad (10)$$

Now the summation runs from 1 to 6.

At equilibrium, the tensor $\tau$ should be zero. In the calculations, we have always taken the experimental geometry as the starting point for the elastic energy expansion. In AlAs, the calculated minimum energy is obtained for the experimental geometry. However, for CdTe, the energy minimum is obtained for a value of the lattice parameter which is different from the experimental value by 2.4%. It results in the existence of the nonvanishing values for the tensor $\tau$.

In order to determine the three elastic constants of the cubic AlAs and CdTe lattices we have employed the following two independent deformations: Case (i),

$$e_3=-\varepsilon ,$$
$$2e_1=2e_2=\varepsilon , \quad (11)$$

and case (ii)

$$e_6=2\varepsilon .$$

In the above two deformations the unit-cell volume of the crystal has been kept unchanged. Case (i) determines the value of the combination $(C_{11}-C_{12})$ whereas case (ii) gives $C_{44}$. The third constraint is the evaluation of the bulk modulus $B=\frac{1}{3}(C_{11}+2C_{12})$. These three equations are able to give the values of $C_{11}$, $C_{12}$ and $C_{44}$, separately.

## III. CALCULATION AND RESULTS

In the present calculation, the basis employed for making expansions of the products of the LMTO envelopes includes functions with $l\leq 4$ and of energies $-0.01$, $-1.0$, and $-2.3$ Ry and with decay given by $\lambda^2=-1$ and $-3$ Ry. The set will include 50 functions for each atomic sphere. The local density potential of Hedin and Lundqvist has been employed. An absolute convergence to better than 1.0 mRy/atom is obtained with *spd* basis of 22 LMTo's for each atom. The number of atoms in the unit cell was taken to be four.

The muffin-tin (MT) spheres were chosen to be slightly smaller than touching and the radii for cation and anion in each compound were chosen to be equal. The values of the radii of spheres for AlAs and CdTe were taken as 2.22 and 2.54 a.u., respectively.

An equal number of empty spheres of sizes equal to cation or anion were introduced in the vacant interstitial positions available in the zinc-blende structure.

### A. Electronic structure

A two panel calculation was performed for each substance to investigate the important role (usually not appreciated) played by the semicore $3d$ and $4d$ states. In AlAs, in the first panel we consider Al($3s,3p,3d$) and As($4s,4p,4d$) as valence states whereas, in the second panel, we consider almost completely filled As($3d$) states as the semicore ones. Similarly in CdTe, in the first panel Cd($5s,tp,4d$) and As($5s,5p,5d$) states are taken as the valence states, and in the second panel As($4d$) states are assumed to be the semicore states. A set of appropriate ( *spd* ) states were also included on all the empty spheres. The semicore As($3d$) and Te($4d$) electrons are thus treated as bands in a way similar to valence electrons. The core electrons are treated not in the frozen-core approximation but are allowed to relax. This means that the core-electron charge density is recalculated in each iteration in the self-consistency loop.

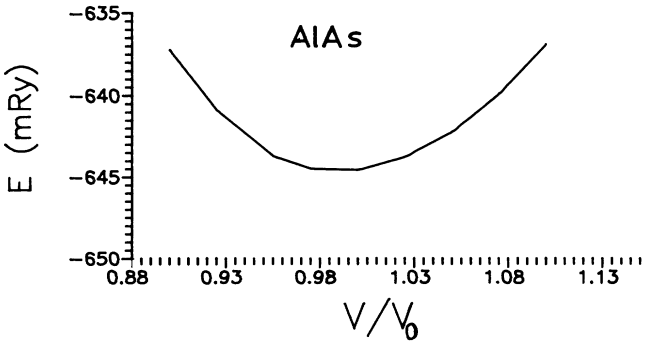


FIG. 1. Variation of crystal energy (in units of milliRydberg) with the ratio of unit-cell volumes $V_0$ and $V$ are th experimental and calculated volumes for AlAs.

In all the calculations, the relativistic effects have been included. The variation of the total electronic energy with the volume of the crystal $V$ has been shown in Figs. 1 and 2, $V_0$ being the experimental volume of the solid. For AlAs (Fig. 1), the energy minimum appears at a value of the lattice parameter equal to 5.66 Å which is just equal to the experimental value.[5] On the other hand, for CdTe (see Fig. 2), the energy minimum appears at $a=6.32$ Å (experimental value[5] is 6.48 Å) which shows a deviation of approximately 2.4%.

The charge out of the muffin-tin sphere, i.e., the difference between the atomic number and the charge lying within the MT sphere for the atoms Al, As, Cd, and Te is 1.71, 1.85, 1.52, and 2.30 electron charges ($e$), respectively. The total charge per unit cell outside the MT spheres is 2.87$e$ in AlAs and 3.16$e$ in CdTe.

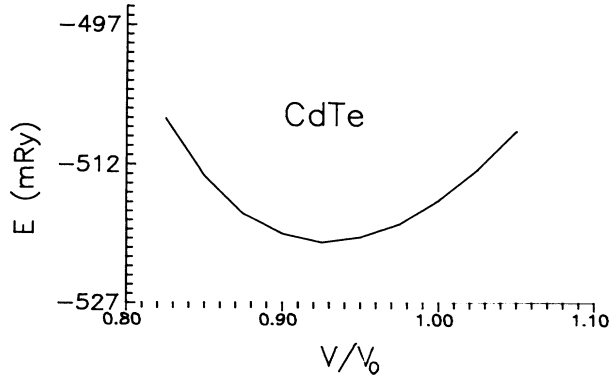


FIG. 2. Same as for Fig. 1 except for CdTe.

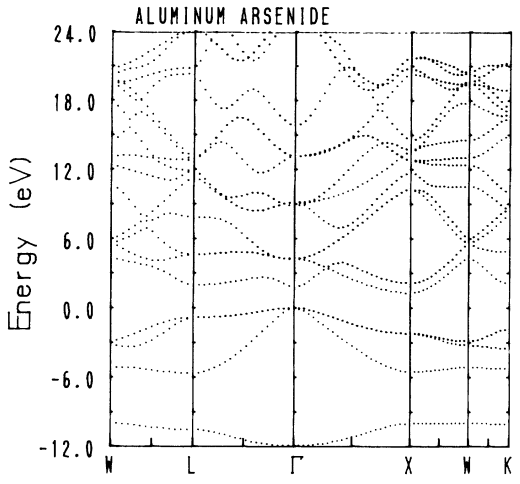


FIG. 3. Dispersion curves for AlAs.

### 1. AlAs

The calculated dispersion curves along some important symmetry directions for AlAs are shown in Fig. 3. The symmetry points are Γ (0,0,0), $X$ (1,0,0), $K$ (0.75,0.75,0.0), $L$ (0.6,0.6,0.6), and $W$ (1.0,0.5,0.0).

In AlAs (Fig. 3) at the most symmetric Γ (0,0,0) point, the lowest valence state at −11.9 eV is the bonding Al($3s$)-As($4s$) singlet. The top of the valence band which has been set at zero energy is formed by the triply degenerate hybridized Al($3d$)-As($4p$) orbitals. The conduction state appearing at 1.8 eV is the antibonding Al($3s$)-As($4s$) singlet state. The higher conduction states are formed by the hybridization of the Al($3p$,$3d$) and As($4p$,$4d$) in an antibonding manner.

At the symmetric point $X$(1,0,0), the low-lying singlet valence states have bonding character and are composed of the Al($3p$)-As($4s$), Al($3s$)-As($4p$), and Al($3p$)-As($4p$) states. The conduction states have the same nature except that they have the antibonding character. Their occurrence in the energy scale is similar to the valence states. The semicore As $3d$ states lie quite below near −34.3 eV.

In the calculation of the electronic density of states (DOS), a sampling method with Gaussian broadening of energy 0.2 eV was employed over a mesh of 19 points in the irreducible part of the Brillouin zone. The calculated DOS for the self-consistent calculation for AlAs is shown in Fig. 4. The valence-band states are distributed over an energy interval of 11.9 eV. The lowest peak at −11.9 eV arises from the Al($3s$,$3p$) and As($4s$) orbitals which posses a bonding character. The other main peaks appearing at −5.2, −3.2, −2.3, and −1.6 eV are comprised of the Al($3s$)-Al($4p$), Al($3p$)-As($4p$), and Al($3d$)-As($4p$) having antibonding character. The top of the valence band is formed by the bonding states of the $3d$ states of Al and $4p$ states of As. The bottom of the conduction band is formed by the antibonding Al($3p$) and As($4s$) states. The other peaks in the conduction states originate from the antibonding states Al($3s$)-As($4p$), Al($3s$)-As($4p$), Al($3p$)-Al($4p$), Al($3d$)-As($4d$), etc. The calculated energy gap is an indirect one and its value of 1.31 eV is quite small as compared with the experimental value of 2.3 eV. This behavior of obtaining a reduced value for the energy gap has always been seen in all calculations using the local-density-functional theory. Thus the calculated conduction states seem to be reliable in their character, although their overall location may be shifted somewhat towards the low-energy side by a magnitude equal to the difference between the experimental and the calculated values of the energy gap. We are not aware of any photoemission data available for AlAs for comparison.

Contour plots of the self-consistent valence charge density for AlAs in the $(1\bar{1}0)$ plane is shown in Fig. 5. The contours are plotted in steps of $0.005e$ a.u.$^{-3}$ up to a

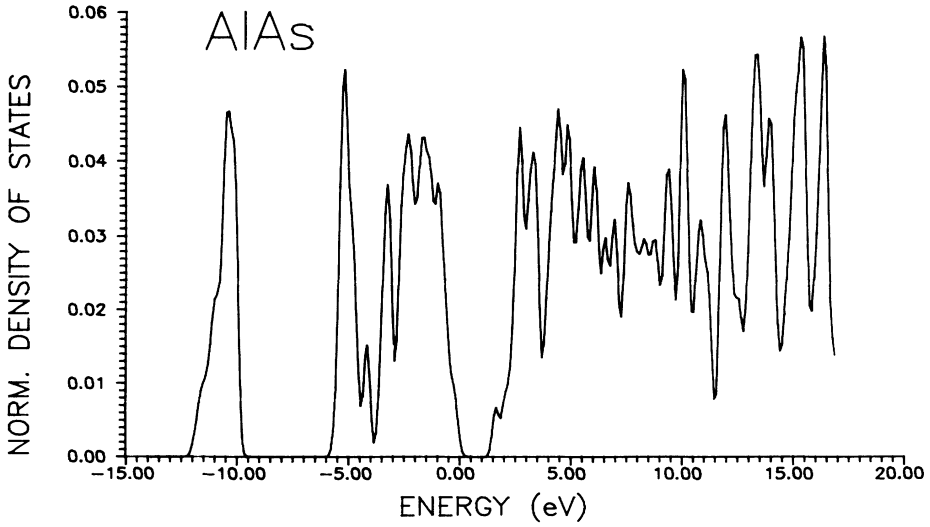


FIG. 4. Electronic density of states for AlAs.

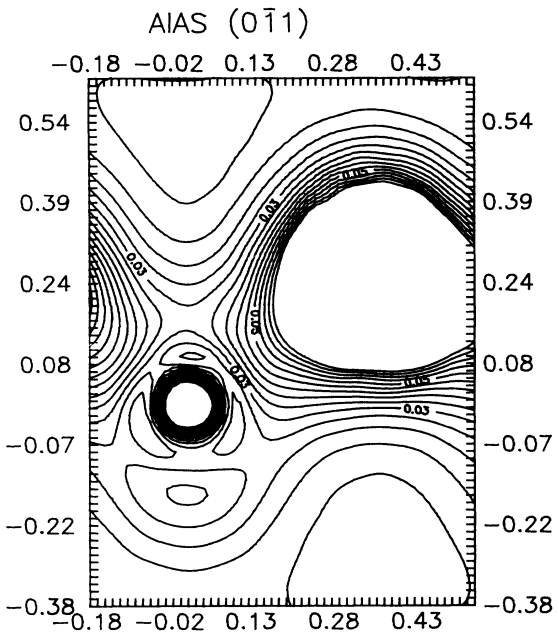


FIG. 5. Contour plots of the self-consistent charge density for the (1$\bar{1}$0) plane of AlAs. The plots are in steps of 0.005$e$ a.u.$^{-3}$ up to a maximum of 0.07$e$ a.u.$^{-3}$.

maximum of 0.07$e$ a.u.$^3$. The bonding between Al and As atoms reveals a mixed character.

### 2. *CdTe*

The computed dispersion curves for the electron states are depicted in Fig. 6. At Γ (0,0,0), similar to AlAs, the lowest valence states are composed of the singlet bonding Cd(5$s$)-Te(5$s$) orbitals with dominant contribution from Te(5$s$) states. The next higher triply and doubly degenerate valence states arise mainly from the Cd(4$d$) orbitals with some mixing with the Te(5$p$) orbitals. The top of the valence band originates from the Te(5$p$) orbitals possessing triply degenerate character. The bottom of the conduction band appearing at 0.75 eV is comprised of the antibonding 5$s$ states of Cd and Te atoms. The results are in agreement with those of Wei and Zunger.[6]

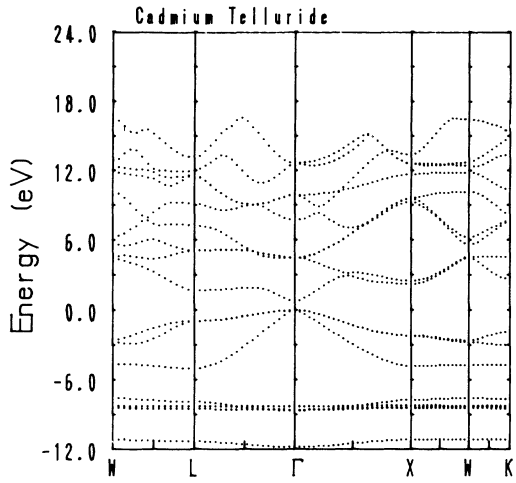


FIG. 6. Dispersion curves for CdTe.

AT the $X$ point extra valence states appear either from the bonding Cd(5$s$)-Te(5$p$) orbitals or from the Cd(5$p$)-Te(5$p$) orbitals next below the valence-band edge. Again the semicore Te(4$d$) states appear much below around −36.1 eV.

The total DOS for CdTe is shown in Fig. 7. The valence-band states appear in an energy interval of 11.8 eV. The major peaks in the valence states region appearing at −11.2, −8.3, −4.8, −2.8, −2.1, −1.6, and −1.0 eV originate mainly from the antibonding

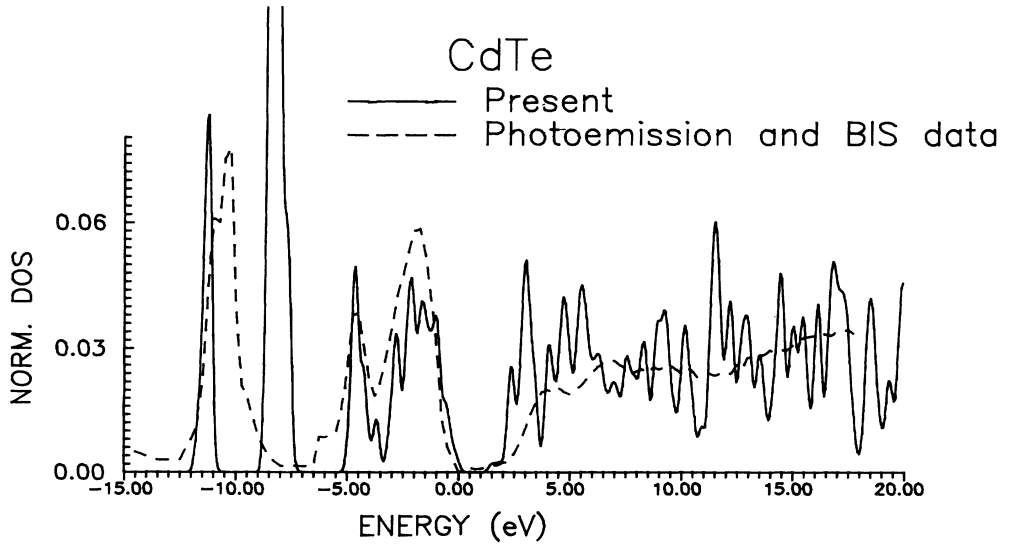


FIG. 7. Electron density of states for CdTe.

Cd($5s,5p$)-Te($5s$), Cd($4d$), Cd($5s$)-Te($5p$), and Cd($5p$)-Te($5p$) states, respectively. A number of peaks in the conduction-band region arise from the similar mixed states but possessing antibonding character. The calculated energy gap of 0.75 eV is quite small as compared to the experimental values of 1.56 eV.

Recently, the photoemission data and the bremsstrahlung-isochromat-spectroscopy (BIS) data determining respectively the occupied and the unoccupied states for a single crystal of CdTe are available.[8] We have compared them with the computed DOS in Fig. 7.

In the valence state region, one observes a double peak structure at $-11.0$ and $-10.5$ eV, two peaks near $-4.5$ and $-1.5$ eV and two shoulders near $-9$ and $-3$ eV. The calculated main peaks around $-11.2$, $-8.3$, $-4.6$, $-3.7$, and $-2$ eV are quite close to the experimental data. In fact, the calculated DOS if shifted towards the higher energy side by about 0.5 eV is in excellent agreement with the measured data. The only important discrepancy lies in the appearance of a double peak structure around $-10.5$ eV. However, the x-ray photoemission spectra (XPS) of Kowalczyk *et al.*,[8] does not reveal any such double peak structure.

Coming to the unoccupied states, the calculated fine structure is again in very good agreement with the BIS data. For example, the calculated peaks appearing at 2.5, 3.0, 4.0, 4.7, 5.5, 7.0, 9.0, 10.25, 11.5, 11.75, 12.5, 14.5, and 17 eV, etc., are in very close agreement with the BIS peaks at 4.0, 4.5, 6.2, 7.0, 9.5, 10.25, 11.25, 11.75, 12.5, 14.0, 16.5, and 17.5 eV, etc. The only discrepancy is the occurrence of the theoretical peaks near 3 eV which have not been seen in the experiments.

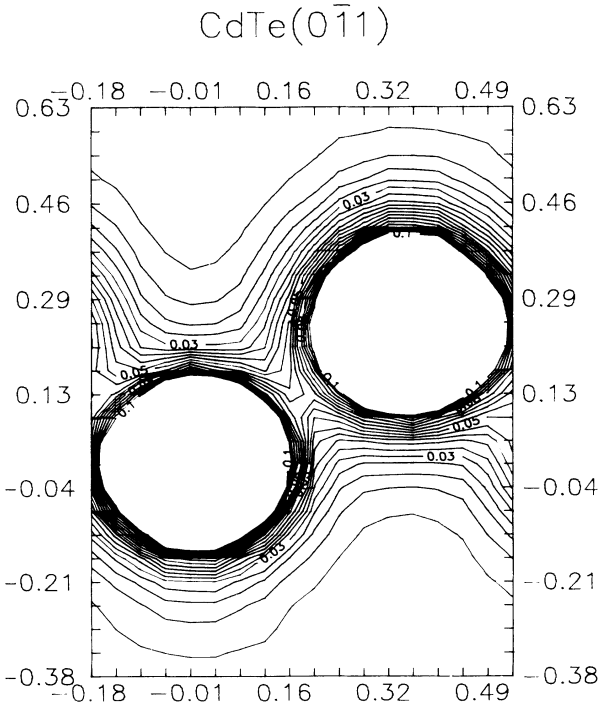


FIG. 8. Same as for Fig. 5 but for CdTe.

TABLE I. Computed physical quantities for AlAs. The elastic data are in units of mbar whereas the phonon frequencies are in $cm^{-1}$.

| Sample number | Quantity | Present | Expt. |
|---|---|---|---|
| 1 | Bulk modulus $B$ | 0.70 | |
| 2 | $C_{11}$ | 1.15 | |
| 3 | $C_{12}$ | 0.477 | |
| 4 | $C_{44}$ | 0.68 | |
| 5 | LTO($\Gamma$) | 372 | 372[a] |
| 6 | LAO($X$) | 334 | |
| 7 | $TO_1(X)$ | 368 | |
| 8 | $TO_2(X)$ | 221 | |
| 9 | TA($X$) | 126 | |

[a]Reference 10.

Contour plots of self-consistent valence charge density for CdTe in the $(1,\bar{1}0)$ plane are shown in Fig. 8. The contours are plotted in steps of $0.003e$ a.u.$^{-3}$ up to a maximum of $0.07e$ a.u.$^{-3}$. The bonding between Cd and Te atoms reveals a mixed character.

### B. Elastic constants

For the evaluation of the energy derivatives, we have used five different values of $\varepsilon$. The maximum value of $\varepsilon$ is taken as $\pm 0.04$. The change in the internal energy given by Eq. (10) is fitted to polynomials of order 0,2, and 3 and the coefficients of the various polynomials are evaluated which are equal to some multiple of the different combinations of the elastic constants.

The results for the elastic constants for AlAs and CdTe are included in Tables I and II, respectively, which also contain the experimental data wherever available. No elastic data are available for AlAs. For CdTe, the presently computed values for the bulk modulus, $C_{11}$ and $C_{12}$, are in very good agreement with the experimental values.[9] However, for $C_{44}$, the calculated value of

TABLE II. Computed physical quantities for CdTe. The elastic data are in units of mbar whereas the phonon frequencies are in $cm^{-1}$.

| Sample number | Quantity | Present | Expt. |
|---|---|---|---|
| 1 | Bulk modulus $B$ | 0.417 | 0.445[a] |
| 2 | $C_{11}$ | 0.532 | 0.535[b] |
| 3 | $C_{12}$ | 0.360 | 0.368[b] |
| 4 | $C_{44}$ | 0.318 | 0.199[b] |
| 5 | LTO($\Gamma$) | 165 | 167(LO)[c], 167 (TO)[c] |
| 6 | LAO($X$) | 165 | 152[d] |
| 7 | $TO_1(X)$ | 130 | |
| 8 | $TO_2(X)$ | 114 | |
| 9 | TA($X$) | 52.5 | 36[e] |

[a]Reference 14.
[b]Reference 9.
[c]Reference 11.
[d]Reference 12.
[e]Reference 13.

0.318 mbar is much higher than the experimental value 0.199 mbar. The large difference in the experimental values of $C_{12}$ and $C_{44}$ is somewhat unexpected keeping in view the observed values for those elastic constants for other substances.

### C. Phonon frequencies

The variation of the internal energy with different types of static deformations in the small deformation limit can be utilized for the determination of some of the frozen symmetry points of the Brillouin zone. Calculations have been performed for the longitudinal-transverse-optical mode at the $\mathbf{k}=\mathbf{0}$ ($\Gamma$) point and the longitudinal-acoustical-optical (LAO), transverse-optical (TO), and transverse-acoustical (TA) modes at the point $X$ (100). The transverse-optic mode splits because of the motion of the single atom in the mode, each atom possessing different mass. The results for AlAs and CdTe have been included in Tables I and II, respectively.

For AlAs, (see Table I) the only available data[10] are for the transverse-optical mode $\mathbf{k}=\mathbf{0}$ ($\Gamma$) and are equal to 372 $cm^{-1}$ which is in agreement with the presently calculated value of 372 $cm^{-1}$.

For CdTe (see Table II), the calculated frequencies are in close agreement with the available experimental data[11–13] keeping in view the complicated distortion involved in these phonon modes and the complexity of the total energy calculation in the local-density formulation and the inherent uncertainty in measurements. The agreement seems to be satisfactory.

## IV. CONCLUSIONS

The modified version of the first-principles full-potential self-consistent LMTO method has the capacity to predict most of the physical quantities which are in very good agreement with the experiments both in a qualitative and quantitative manner. The application of the method to the representative of the III-V and II-VI semiconducting compounds AlAs and CdTe and the comparison of the computed data with the available data are seen to support this statement.

## ACKNOWLEDGMENTS

The authors express their thanks to M. Methfessel for allowing use of the code and for useful discussions. All the calculations were performed on a MicroVaxII system available to us. The financial assistance from University Grants Commission, New Delhi, and Department of Science and Technology, New Delhi, are acknowledged.

[1]M. Methfessel, Phys. Rev. B **38**, 1557 (1988).
[2]M. Methfessel, C. O. Rodriguez, and O. K. Anderson, Phys. Rev. B **40**, 2009 (1989).
[3]M. M. Polatoglou and M. Methfessel, Phys. Rev. B **41**, 15 898 (1990).
[4]M. Methfessel, Bal K. Agrawal, and M. Scheffler, (unpublished).
[5]*CRC Handbook of Chemistry and Physics,* 70th ed. (Chemical Rubber, Boca Raton, Fl, 1990).
[6]S. H. Wei and A. Zunger, Phys. Rev. B **37**, 8958 (1988).
[7]A. Wal, Y. Gao, A. Raisanen, A. Franciosi, and J. R. Chelikowsky, Phys. Rev. B **43**, 4988 (1991).
[8]S. P. Kowalczyk, J. T. Cheung, E. A. Kraut, and R. W. Grant, Phys. Rev. Lett. **56**, 1605 (1986).
[9]H. J. McSkimm and D. G. Thomas, J. Appl. Phys. **33**, 56 (1962).
[10]M. Ilegems and G. L. Pearson, Phys. Rev. B **1**, 1576 (1970).
[11]R. Beserman and M. Balkanski (private communication).
[12]A. Mooradian and G. B. Wright, in *IX International Conference on Physics of Semiconductors,* edited by S. M. Ryvkin (Nauka, Leningrad, 1968), p. 1020.
[13]G. A. Slack and S. Roberts, Phys. Rev. B **3**, 2613 (1971).
[14]*Numerical data and Functional Relationships in Science and Technology,* Landolt-Börnstein, Vol. 17b, edited by O. Madelung (Springer Verlag, Berlin, 1982).